Journal of
Micro/Nanolithography,
MEMS, and MOEMS

Nanolithography.SPIEDigitalLibrary.org

Magnetic debris mitigation system for extreme ultraviolet sources

Daniel T. Elg
John R. Sporre
Davide Curreli
Ivan A. Shchelkanov
David N. Ruzic
Karl R. Umstadter

SPIE.

Magnetic debris mitigation system for extreme ultraviolet sources

Daniel T. Elg,[a] John R. Sporre,[a,†] Davide Curreli,[a] Ivan A. Shchelkanov,[a] David N. Ruzic,[a,*] and Karl R. Umstadter[b]
[a]University of Illinois at Urbana-Champaign, Center for Plasma-Material Interactions, Department of Nuclear, Plasma, and Radiological Engineering, 216 Talbot Laboratory MC-234, 104 South Wright Street, Urbana, Illinois 61801, United States
[b]KLA-Tencor Corporation, 1 Technology Drive, Milpitas, California 95035, United States

Abstract. In extreme ultraviolet (EUV) lithography, plasmas are used to generate EUV light. Unfortunately, these plasmas expel high-energy ions and neutrals which damage the collector optic used to collect and focus the EUV light. One of the main problems facing EUV source manufacturers is the necessity to mitigate this debris. A magnetic mitigation system to deflect ionic debris by use of a strong permanent magnet is proposed and investigated. A detailed computational model of magnetic mitigation is presented, and experimental results from an EUV source confirm both the correctness of the model and the viability of magnetic mitigation as a successful means of deflecting ionic debris. [DOI: 10.1117/1.JMM.14.1.013506]

Keywords: extreme ultraviolet; collector; debris mitigation; magnetic mitigation; ionic debris.

Paper 14117P received Jul. 21, 2014; accepted for publication Jan. 12, 2015; published online Feb. 9, 2015.

1 Introduction

Moore's law states that the number of transistors on a die must double every 2 years.[1] By following this law, the semiconductor industry has managed to produce integrated circuits with a feature size of 22 nm at the present time.[2] Further extension of Moore's law will require this size to shrink even more. However, current lithographic techniques create integrated circuits by employing 193 nm lasers to create patterns on Si wafers. Techniques such as immersion lithography and double patterning have allowed manufacturers to etch feature sizes smaller than the current wavelength.[3] Unfortunately, these techniques become more complex and costly every time the feature size is decreased. For this reason, it is desirable to enable further reduction in feature size by using a smaller wavelength of light.

Extreme ultraviolet (EUV) lithography allows for this by making use of 13.5-nm light, and it holds great promise as a next-generation lithography technique. Unfortunately, many differences with conventional lithography have caused problems which have, thus far, kept EUV from being cost-effective. Due to the high energy of EUV photons, EUV must be created by a dense, energetic plasma ($T_e \sim 30$ eV, $n_e \sim 10^{19}$–10^{21} cm^{-3}) rather than a laser.[4,5] Since all known window and lens materials absorb EUV, the light must be collected and focused by a collector mirror that is directly exposed to the plasma. However, the plasma expels high-energy ions and neutrals. These can damage the collector optic by coating it and lowering its EUV reflectivity. High-energy ions also have the potential to cause sputtering or implantation.[6] When a collector is damaged, it must be cleaned or replaced, which causes system downtime and raises the cost-of-ownership for an EUV source.

To mitigate ionic debris, the use of magnetic mitigation has been investigated at the Center for Plasma-Material Interactions (CPMI) at the University of Illinois at Urbana-Champaign. The main point of this paper is to measure and model the effects of magnetic mitigation, especially with regard to potential applications in EUV metrology sources. After performing basic simulations to determine the range of field magnitudes required for significant deflection, a useful magnet topology has been chosen. The magnet has been modeled in COMSOL, and a MATLAB® simulation has been written to predict the trajectories of energetic ions under the influence of the magnet. The system simulated in MATLAB has been implemented inside an XTS 13-35 EUV source located at CPMI. An electrostatic analyzer (ESA) was used to quantify the ion debris flux at multiple locations on the source. The ion energy distribution functions (IEDFs) seen on the ESA are in agreement with those predicted by the simulation. Previous industrial research[7,8] has shown that magnetic fields can cause significant decreases in ion fluxes at certain individual points in space. However, such research has not predicted or shown measurements of the locations to which ions of various energies are deflected. In this paper, angular deflected ion energy distributions are predicted and measured. The model described herein can be used to predict the deflection of ions of various energies in any quantifiable EUV source and for any magnetic field structure. Additionally, the particular magnetic mitigation system described in this paper is especially relevant for potential use in EUV metrology sources.

2 Experimental Setup

2.1 *Extreme Utraviolet Source*

CPMI is home to an Xtreme Technologies XTS 13-35 EUV source. This z-pinch discharge-produced plasma source was originally designed to produce 35 W of EUV by using Xe as the pinch gas.[9] However, due to the high cost and low accessibility of Xe, the experiments in this paper used Ar as the

*Address all correspondence to: David N. Ruzic, E-mail: druzic@illinois.edu

†Present address: IBM Corporation, 257 County Road 156, Albany, New York 12203, United States

0091-3286/2015/$25.00 © 2015 SPIE

pinch gas. While Ar does not produce EUV, EUV production was not necessary for proof-of-concept magnetic mitigation experiments. The XTS 13–35 is designed to create a plasma with a temperature of approximately 30 eV.[10] The high ion energies seen in the XTS 13–35 (on the order of keV) are due to ion acceleration by an electric field, which is set up by a space charge imbalance caused by electrons initially leaving the core plasma more quickly than ions[11] This phenomenon will occur for any gas used to fuel the z-pinch, accelerating ions to energies on the order of keV. An Ar pinch of comparable electron temperature and electron density would also expel debris of energies on the same order as an Xe pinch, and it was this high-energy debris that was necessary for the experiments and modeling in this paper.

The XTS 13–35 is attached to the Xtreme commercial EUV exposure diagnostic (XCEED) chamber. XCEED is equipped with two turbo pumps and a roughing pump, allowing the base pressure to be lowered to approximately 2×10^{-6} Torr. During experiments, an Ar flow rate of approximately 440 sccm and an operating pressure of 3 mTorr were used. The pinch frequency was set to 20 Hz. For better experimental control, no buffer gas was used.

XCEED is also equipped with a series of angular ports which are at the same vertical height as the pinch. As shown in Fig. 1, these ports allow for a direct line of sight to the pinch from 0 deg (head-on) as well as from angles in 5 deg increments between 15 deg and 45 deg.

2.2 *Electrostatic Energy Analyzer*

The ionic output of the source is measured with a spherical-sector ESA. The particular ESA used in these experiments is a Comstock AC-902B. The construction, operation, and principles of this ESA are described in detail in Ref. 12. The ESA can be attached to XCEED at any angular port. A laser is used in conjunction with a bellows to make sure the ESA is aligned with a line of sight to the pinch. An example diagram with the ESA attached to the 0 deg port is shown in Fig. 1. The "Approximate Location of B-Field" refers to the eventual location of the magnet used for the experiments detailed in this paper; details about the magnet topology, size, and position will be given in Sec. 3.

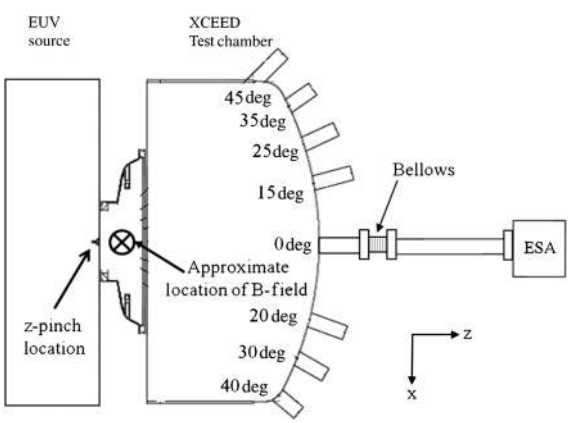

Fig. 1 A top-down drawing of the extreme ultraviolet (EUV) source, Xtreme commercial EUV exposure diagnostic (XCEED) chamber, and electrostatic analyzer (ESA) chamber is shown. Ions are emitted from the z-pinch location. XCEED is equipped with various angular ports, all of which have a direct line of sight to the z-pinch. The ESA chamber can be attached to any port for the purposes of measuring the ion flux at that port. In this diagram, the ESA chamber is attached to the 0 deg port via a nipple and bellows. It is aligned by aiming a laser at the center of the pinch. For the experiments shown in this paper, a magnet was placed at the "Approximate Location of B-Field." The magnet topology, location, and size will be detailed in Sec. 3 of this paper.

The ESA functions as an energy-to-charge selector. Ions with the desired energy-to-charge ratio are incident on a set of multichannel plates (MCPs) which output an electrical signal. Since most ions from the XTS 13-35 are singly ionized,[11] the ESA essentially functions as an energy selector. The length from the pinch to the MCPs is known to be approximately 1.65 m. Since the energy E is set by the ESA, time of flight t is recorded by the oscilloscope, and flight path length l is known, the well-known equation for kinetic energy can be solved for mass in terms of known quantities

$$m = 2E\left(\frac{t}{l}\right)^2. \tag{1}$$

Thus, hits that occur at different times can be attributed to the appropriate masses. The ESA can be tuned to various energies in the range of 0.5–14 keV. By selecting multiple energies and solving Eq. (1), a spectrum of hits versus energy can be found for any desired mass. As described in Ref. 12, these hits can be converted into ion fluxes by means of Eq. (2),

$$f = \frac{N * C}{2 * A * p * \Delta E}, \tag{2}$$

where N is the number of hits, C is the calibration factor, A is the ESA entrance orifice area, p is the number of pinch pulses recorded, and dE is the energy resolution of the ESA at the selected energy. The diameter of the ESA orifice is 2 mm, and the number of pulses recorded at each energy is 2400 (2 min of operation at 20 Hz). The calibration factor and energy resolution ΔE are calculated through methods shown in Ref. 12.

3 Theory and Magnet Choice

Magnetic mitigation is governed by the following three equations:

$$v = \sqrt{\frac{2E}{m}}, \tag{3}$$

$$\mathbf{F} = q\mathbf{v} \times \mathbf{B}, \tag{4}$$

$$F = m\mathbf{a}. \tag{5}$$

An ion with energy E will have a velocity v. Under a magnetic field, the ion will experience a force dependent on its charge q, its velocity, the magnetic field B, and the angle between $\mathbf{v}$ and $\mathbf{B}$. This force will create an acceleration from which the ion's trajectory can be determined.

To guide the design and choice of the magnet, simple preliminary MATLAB simulations were run in order to obtain an estimate of the field magnitude necessary for significant deflection of 10 keV Ar^+ ions. These preliminary simulations assumed a uniform magnetic field existing in a circular

region 10 cm in diameter, which corresponded to a size that would fit in the XCEED chamber. The results indicated that, for such a magnet, a field greater than 0.5 T would be necessary.

COMSOL modeling showed that, for these high fields, a conventional electromagnet of reasonable size was out of the question. Due to the low field strength of conventional electromagnets and the high cost of superconducting electromagnets, a Halbach array was chosen to provide the field.

A Halbach array is an arrangement of permanent rare-earth magnets structured such that the magnetic fields add to a large value in a certain region and cancel each other in other regions.[13] For this application, a cylindrical Halbach array was used. The outer diameter of the cylinder was 8.62 cm, the inner diameter was 2.54 cm, and the thickness was 2.54 cm. The array consisted of 12 permanent magnets arranged such that the field in the center bore was approximately 0.9 T. A diagram of the Halbach array with individual magnet polarities is shown in Fig. 2(a). The array was modeled in COMSOL in order to accurately determine the field strength and direction in three-dimensional (3-D) space. The COMSOL model with field lines is shown in Fig. 2(b). The field in the center bore (Region 1) is strong and points mostly in the $-y$-direction. Inside the physical boundaries of the array (Region 2), the field is irrelevant because ions cannot travel through the walls of the array. The field is weak in other regions outside the physical boundaries of the array (Region 3). These results confirm that the Halbach array model is behaving as expected for a Halbach array. In this model, the x-direction is horizontal, the y-direction is vertical, and the z-direction points out of the page. The array was oriented to obtain the maximum in-bore field contribution in the $-y$-direction.

The Halbach array was mounted inside XCEED so that the Halbach array and the z-pinch were coaxial, with the z-axis passing through the center of the Halbach array orifice [Region 1 in Fig. 2(a)]. The positive z-axis points into the page in Fig. 2, and the center of the array was located 5 cm in front of the pinch. The axes shown in Fig. 2 are the same as shown in Fig. 1; thus, if the origin is assumed to be the center of the Halbach array, the pinch was located at (0, 0, −5 cm). As in the model, the field in the bore was oriented in the negative y-direction; hence, ions ejected in the positive z-direction by the pinch were deflected in the negative x-direction toward the odd-numbered ports in Fig. 1, according to Eq. (4). The approximate location of the magnetic field is shown in Fig. 1. In other words, the Halbach array and z-pinch were coaxial, with the center of the Halbach array placed 5 cm in front of the pinch. The size of the Halbach array orifice [Region 1 in Fig. 2(a)] and position of the array allowed for an 11.45 deg half-angle of view from the pinch. Though this does block some light, such a system could be very useful in an actinic inspection source, which requires a high brightness in a small area, rather than a high level of EUV power at any angle.[14]

4 Simulation

To predict the trajectories of ions, it was necessary to model the XTS 13–35 source and then solve the ion equations of motion [Eqs. (3) to (5)] quickly enough to run hundreds of thousands of ion flights. The underlying goal of the simulation was to predict deflected IEDFs at various ports on XCEED; these IEDFs could then be experimentally measured with the ESA. Due to the velocity-dependent magnetic force in Eq. (4), it was expected that different angular ports would see different energy distributions of deflected ions.

4.1 *Initial Velocities*

To provide a reliable simulation of ion trajectories, the ejection of ions from the source must first be modeled. The XCEED pinch is approximately 3 mm in diameter. This small size allows for the pinch to be modeled as a point source. The initial velocity of all ions comprised two components:

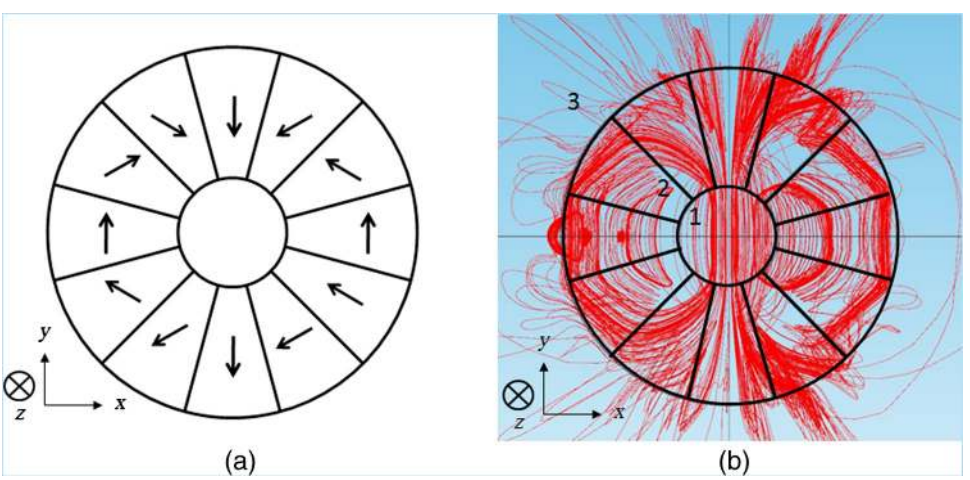

Fig. 2 (a) A cylindrical Halbach array is diagrammed. In this case, the array is made up of 12 magnets. The magnetization vectors of each magnet are shown by the arrows, creating a field that is strong in the center bore and weak outside the outer diameter of the array. (b) The Halbach array used in this paper was modeled in COMSOL. The dimensions are: OD 8.62 cm, ID 2.54 cm, and thickness 2.54 cm. The axis of the array is coincident with the z-axis and coaxial with the z-pinch. The pinch is located on the z-axis 5 cm behind the Halbach array. Inside the center bore of the magnet (Region 1), the field is strong and points almost completely in the $-y$ direction, producing a field magnitude of 0.9 T at the origin. Outside the physical boundaries of the array, the field is comparatively weak (Region 3). The field inside the array's physical boundaries (Region 2) is irrelevant because ions cannot travel inside the array.

thermal velocity and drift velocity. As is typical for discharge-produced EUV sources, the XTS 13–35 is designed to produce a plasma with electron and ion temperatures of approximately 30 eV.[10] In the simulation, a Maxwellian distribution centered at 30 eV is used to determine a simulated ion's thermal velocity, which is applied in a random direction.

The other component, drift velocity, is caused by the fact that 30 eV electrons have much higher velocities than 30 eV ions. The fast electrons leave the plasma faster than the ions, creating a spatial charge imbalance. This charge imbalance gives rise to an electric field, which accelerates ions out of the pinch at drift velocities that are much higher than the ions' thermal velocities.[11] The drift velocity, on the order of keV, is responsible for most of an ion's kinetic energy. In the simulation, it is modeled as a velocity that points straight out of the point source along the z-axis. Thus, the initial velocities of simulated ions contain large z-components, with an angular spread about the z-axis provided by the thermal component.

In the simulation, assigned drift velocities are based on a measured ion energy distribution. Without the magnet present, the ESA is used to measure an experimental IEDF at the 0 deg port of XCEED. From the measured IEDF, a normalized cumulative distribution is formed. Drift velocities of simulated ions are selected based on this normalized CDF. In this manner, the actual source output probabilistically influences simulated drift velocities.

4.2 *Ion Trajectories and Energy Distributions*

Given an initial ion velocity, the equations of motion [Eqs. (3) to (5)] must be solved to calculate the ion's trajectory under magnetic mitigation. The 3-D grid of magnetic field values from the COMSOL model was imported into MATLAB. If an ion is inside the COMSOL grid, the magnetic field is set to the **B** value at the nearest grid point; if the ion is outside the grid, **B** is assumed to be 0 T.

The large number of simulated ion flights required to provide a reliable simulation necessitates the use of an ordinary differential equation solver that is quicker than MATLAB's built-in solvers but more accurate than a simple forward-Euler approach. For that reason, a second-order Boris-Buneman solver is implemented. This algorithm, documented in Ref. 15, provides high computation speed while maintaining a reasonable degree of accuracy.

For a desired angular port, a simulated ESA orifice is placed at the point where it would lie in real life given the dimensions of the system. Simulated ions passing through this orifice are counted as "collected," and their energies are recorded. In this way, a simulated IEDF of deflected ions at any desired angular port can be calculated.

As an example, an IEDF was measured at the 0 deg port without the magnet present. The data were then used to produce 5×10^5 simulated ions, which were flown with the field turned off. Ions passing through a simulated ESA orifice at 0 deg were counted. The total simulation time was approximately 1 h. The IEDF of simulated ions was linearly scaled to match the magnitudes of the flux measurements. As shown in Fig. 3, the IEDF of simulated ions shows good agreement with the experimental data, confirming that the method of choosing simulated ion velocities is correctly working. Additionally, measurements of the 0 deg flux were taken with the Halbach array installed. These results, also shown in Fig. 3, indicate that the Halbach array reduces the flux at 0 deg by between 1 and 2 orders of magnitude. The presence of the small remaining ionic fluxes can be attributed to scattering, which is not accounted for in the simulation. Note that the flux at 5 keV is not shown because no flux was distinguishable above the noise threshold at 5 keV. Though these results show that deflection is occurring, a more complete treatment of deflection must include simulations and measurements of the angles by which ions of various energies will be deflected. Such a treatment provides the ability for source manufacturers to determine the angular space which a collector may occupy without being hit by ions of specified energies. This treatment is provided in the next sections.

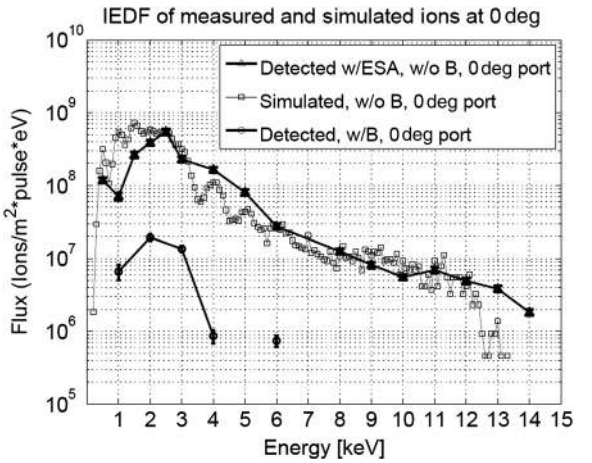

Fig. 3 After measuring an ion energy distribution function (IEDF) at the 0 deg port with the magnet removed, 5×10^5 ions are created by the simulation, with initial drift velocities based on the energies of the measured ions. To test the success of this approach, the simulated ions are flown through a simulated chamber with no magnetic field. Ions reaching a simulated ESA at the 0 deg port are counted and binned into a histogram by energy. This is compared to the original measured IEDF. After scaling the computational flux, the two IEDFs show good agreement. In addition, the flux at 0 deg is reduced by between 1 and 2 orders of magnitude when the Halbach array is present. The presence of the remaining flux can be attributed to scattering, which is not included in the model.

As detailed in Ref. 11, the problem at hand is not that of normal plasma expansion at a given electron temperature. The ions being considered are fast ions accelerated by electric fields to energies on the order of keV, orders of magnitude higher than the original ion and electron temperatures. In such a situation, the effects of many plasma phenomena, such as coulombic ion-ion repulsion, are lessened, and the single-particle approach used in this model becomes reasonable.

5 35 Deg Experiment

To measure deflection, the Halbach array was placed in XCEED and the ESA was attached to the 35 deg port of XCEED. Additionally, the simulation was carried out with the magnet field turned on and a simulated ESA at the 35 deg port. A simulated IEDF was built by recording the simulated ions passing through a simulated ESA at the 35 deg port. The results of the experiment are shown alongside the results of the simulation in Fig. 4.

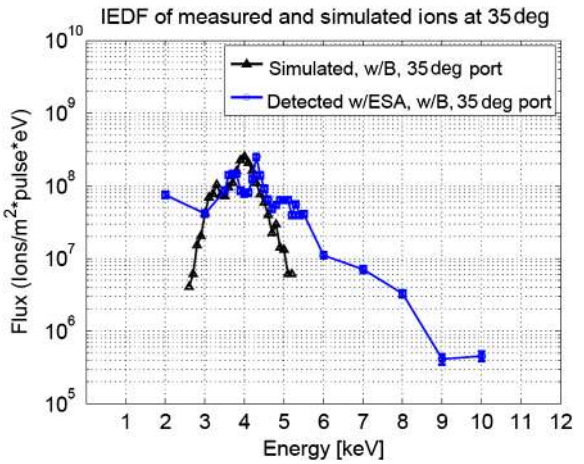

Fig. 4 The deflected ion distribution shown at the 35 deg port follows the simulation rather closely. The flux peak is observed at 4.3 keV, and a secondary peak is observed at 3.7 keV. There is a slight offset on the energy axis because the true field strength at the magnet's center is slightly stronger than the ideal value of 0.9 T used in the model.

It is evident that the experimental data and simulated data show great similarity. The peak experimental deflected flux occurs at 4.3 keV, near the predicted deflected peak of 4 keV. At energies outside of the peak range, the deflected flux is significantly lower than the undeflected flux shown in Fig. 3. Furthermore, the general shape of the measured data seems to mimic that of the simulated data, with a smaller peak being observed at slightly lower energies. The small offset in energy between the simulated and experimental data can be accounted for by the actual magnet being slightly stronger at its center than the ideal 0.9 T value used in the COMSOL simulation.

Outside the peak range, the experimentally measured deflected flux decays sharply, though the decay is not as steep as that predicted in the simulation. This is partly caused by the error inherent in the simulation when the captured flux is at low values; even though 500,000 ions were used in the simulation, not even 100 simulated ions were captured for any given energy outside the peak range. These low simulated captured ion counts give rise to a larger variance and higher errors at energies outside the peak range. Additionally, the shallower decay seen in the experimental data can be attributed to scattering. Scattering is not accounted for in the simulation, and both collisions and Coulombic repulsion can cause ions to deviate from the paths determined for them by the magnetic field. This can give rise to small but higher-than-expected fluxes appearing in the experimental data. Despite this, the simulation and experimental results generally agree with each other to a high degree of fidelity.

It should also be noted that no ion flux was observed at the 0 deg port with the Halbach array in place. Additionally, an experiment was performed to detect any flux at the 35 deg port with no field present. To mimic the physical structure of the mitigation system without providing the magnetic field, a stainless steel dummy of the same dimensions as the Halbach array was built and placed in the mounting system in place of the Halbach array. With this setup, no ion flux was measured at the 35 deg port. These results serve to further confirm that magnetic deflection causes the distribution seen in Fig. 4.

6 45 Deg Experiment

To further confirm deflection, predictions and measurements were also performed at another XCEED port. Because the undeflected flux in Fig. 3 had shown a peak near 2 keV and low-energy ions see greater deflection, the 45 deg port was chosen to try and capture ions in the 2 keV range. After the 35 deg experiment, the z-pinch cathode was replaced. The undeflected flux at 0 with no magnetic field was measured again to account for any potential distribution changes caused by the different electrode. This new IEDF was used as the basis for a simulation of 1×10^6 million ions, which were then flown without the field present and counted by a simulated ESA orifice at the 0 deg port. A comparison of the experimental IEDF and the scaled IEDF of simulated ions, similar to Fig. 3, is shown in Fig. 5. As expected, the two distributions show strong agreement, indicating that the simulation accurately represents the pinch output.

After validating the distribution of simulated ions, the same 1×10^6 million simulated ions were flown with the magnetic field turned on. Experimental deflection was measured by attaching the ESA to the 45 deg port of XCEED with the Halbach array inserted into the chamber. Results comparing the experimental and scaled simulated deflected distributions are shown in Fig. 6.

Deflection is clearly seen in Fig. 6. Though the undeflected IEDF in Fig. 5 does not start decaying until energies higher than 3.5 keV, the deflected IEDF in Fig. 6 begins to rapidly decay beyond the outlier 2.8 keV point. At energies higher than 2.8 keV (and below 1.6 keV), the deflected flux is at least an order of magnitude below the undeflected flux. Additionally, as shown in Fig. 6, the experimental deflected peak energy of 2.2 keV is near the simulated deflected peak energy of 2.4 keV.

The main difference between experiment and simulation is that the experimental data do not seem to drop off steeply until 1.6 keV (on the low end) and 2.8 keV (on the high end),

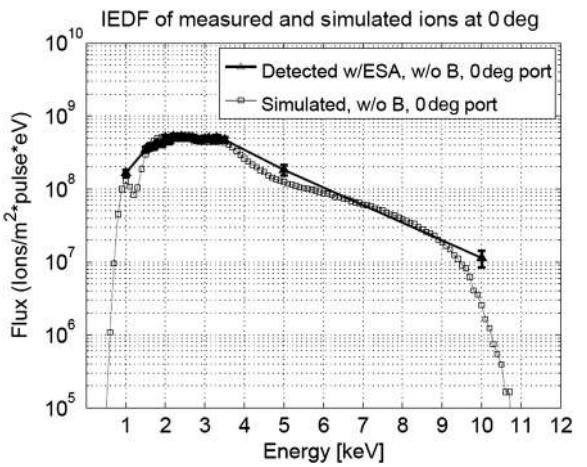

Fig. 5 The cathode was changed after the 35 deg experiment but prior to the 45 deg experiment. In order to account for any change in the distribution caused by this change to the system, an undeflected IEDF was again measured at 0 deg. This IEDF was used to influence initial drift velocities for a simulation of 10^6 ions. To confirm the validity of the simulated drift velocities, these ions were flown with the magnetic field off and were counted by a simulated ESA orifice at the 0 deg port. The experimental data and simulated distributions show good agreement, indicating that the simulated ions accurately represent the output of the pinch.

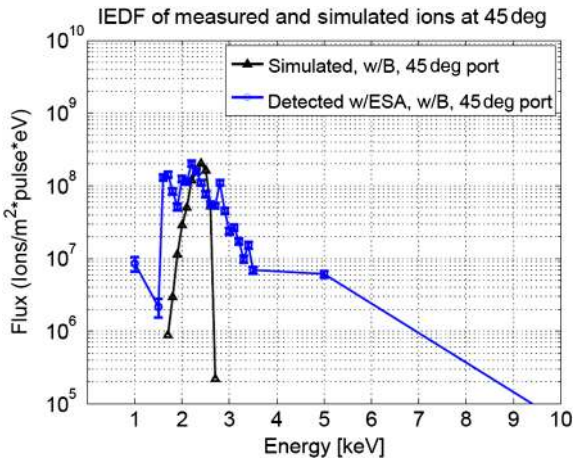

Fig. 6 Experimental data confirm simulation predictions that ions near 2 keV will be deflected to the 45 deg port. At energies higher than 2.8 keV and lower than 1.6 keV, most ions are not deflected to the 45 deg port. The peak of the measured deflected distribution is close to the peak of the simulated deflected distribution. Though the experimental distribution does not decrease as sharply as expected, the model does not account for collisions and coulombic interactions.

while the simulated data show steep drops that begin at energies closer to the peak energy. As previously mentioned, this could be caused by scattering. Additionally, it should be noted that the 2.8 keV point is somewhat of an outlier, being more than a factor of two larger than the points on either side of it. Without this point, the decay would appear much steeper. Nevertheless, the deflected flux still drops away to small values at energies where the undeflected flux remains high. This, combined with the peak location, confirms that deflection is generally occurring as predicted. It should also be noted that the Halbach array mounting apparatus blocks the line of sight between the pinch and the 45 deg port. Though ions passing through the magnet bore can be deflected to the 45 deg port, no ion can travel in a straight undeflected line from the pinch to the 45 deg port.

The modeling and experimentation described in this paper have focused only on predicting the trajectories of the most forward-peaked ions, which reach the 0 deg port when no magnetic field is present. In reality, not all high-energy ions expelled from the source have a drift velocity that is solely in the z-direction; though the z-direction is the most likely direction for a drift velocity, energetic ions are emitted from a z-pinch in a cosine distribution.[16] However, as mentioned in Sec. 3, an EUV metrology source needs only a narrow angle of view to the collector optic, since only the most forward-peaked photons are useful. Since this work was originally motivated by the need for ion mitigation in an EUV metrology source, it was important to predict and measure the deflection of the most forward-peaked ions.

A real EUV metrology source will still likely collect photons from a larger solid angle than that subtended by the ESA orifice in this work. However, since the experiments in this paper have validated the model developed herein, future work can expand the use of the model to predict deflection of ions that are accelerated at angles from the z-axis, allowing source designers to predict the field strength and topology necessary in order to completely deflect ions away from a collector subtending a given solid angle from the source. Additionally, if this approach is expanded to include a wide range of angles, the model detailed in this paper can be used to predict deflection in not only a metrology source, but in any EUV source.

7 Conclusions

A computational model of magnetic mitigation has been developed. This model has been tested by installing a strong permanent magnet in a z-pinch plasma source with characteristics similar to those of an EUV source. The model correctly predicted angular energy distributions of high-energy ions in the source, which were measured with an electrostatic energy analyzer. A deflection of 45 deg was observed for Ar^+ ions between approximately 1.7 and 2.5 keV, and a deflection of 35 deg was observed for Ar^+ ions between approximately 4 and 5 keV. In other words, a collector optic located within 35 deg from the source would be clear of ions below 5 keV, even without any buffer gas. For an optic subtending any given angle from the source, a threshold ion energy could be determined; ions below this energy would not be incident upon the collector.

The mitigation setup described in this paper holds special relevance for EUV metrology sources, which can accommodate a small, strong permanent magnet blocking part of the field of view. However, the model described herein can also be used to predict deflection and angular energy distributions for ions in any magnetic field topology in any EUV source with quantifiable ion fluxes. Though experiments were carried out with Ar for accessibility reasons, the simulation can easily be used to predict trajectories of EUV-producing materials such as Xe or Sn. Additionally, it can be used for any source with measurable ionic output and for any user-specified magnet topology and field strength. Though this model has been demonstrated on a discharge source, it could also easily be used to predict deflection in a laser-produced plasma source as long as the energy distribution of high-energy ions can be measured; such a distribution can be measured with instruments such as the ESA described in this paper. Since high-energy ions can cause not only deposition but implantation and sputtering of the collector, the ability to predict and implement magnetic mitigation holds promise as an important step in developing a cost-effective EUV source.

Acknowledgments

The authors would are grateful for funding and support from KLA-Tencor Corp. Additionally, helpful assistance was provided by undergraduate student Louis Chapdelaine.

References

1. G. E. Moore, "Progress in digital integrated electronics," in *Proc. Int. Electron. Devices Meeting*, Vol. 21, pp. 11–13, IEEE Press, Washington, DC (1975).
2. A. Rahman et al., "Reliability studies of a 22-nm SoC platform technology featuring 3-D tri-gate, optimized for ultra low power, high performance and high density application," in *Proc. Int. Reliability Physics Symp.*, Vol. 51, pp. PI.2.1–PI.2.6, IEEE Press, Monterey, California (2013).
3. Y. Wei and R. L. Brainard, *Advanced Processes for 193-nm Immersion Lithography*, SPIE Press, Bellingham, Washington (2009).
4. B. Huang et al., "Effect of electron density on extreme ultraviolet output of a z-pinch Xe discharge produced plasma source," *Jpn. J. Appl. Phys.* **50**(6S), 06GB09 (2011).
5. R. A. Burdt et al., "Laser wavelength effects on the charge state resolved ion energy distributions from laser-produced Sn plasma," *J. Appl. Phys.* **107**(4), 043303 (2010).

6. J. P. Allain et al., "Debris and radiation-induced damage effects on EUV nanolithography source collector mirror optics performance," *Proc. SPIE* **6586**, 65860W (2007).
7. A. Endo et al., "Laser produced EUV light source development for HVM," *Proc. SPIE* **6517**, 65170O (2007).
8. H. Komori et al., "Magnetic field ion mitigation for EUV light sources," *Proc. SPIE* **5751**, 859 (2005).
9. K. C. Thompson et al., "Experimental test chamber design for optics exposure testing and debris characterization of a xenon discharge produced plasma source for extreme ultraviolet lithography," *J. Microelectron. Eng.* **83**(3), 476–484 (2006).
10. H. Shin et al., "Reflectivity degradation of grazing-incident EUV mirrors by EUV exposure and carbon contamination," *J. Microelectron. Eng.* **86**(1), 99–105 (2009).
11. D. N. Ruzic et al., "Reduction of ion energies from a multicomponent z-pinch plasma," *IEEE Trans. Plasma Sci.* **35**, 606–613 (2007).
12. E. L. Antonsen et al., "Ion debris characterization from a z-pinch extreme ultraviolet light source," *J. Appl. Phys.* **99**, 063301 (2006).
13. K. Halbach, "Design of permanent multipole magnets with oriented rare earth cobalt material," *Nucl. Instrum. Methods* **169**(1), 1–10 (1980).
14. S. Perlitz et al., "Development status and infrastructure progress update of aerial imaging measurements on EUV masks," *Proc. SPIE* **8166**, 816610 (2011).
15. C. K. Birdsall and A. B. Langdon, *Plasma Physics via Computer Simulations*, IOP Publishing, New York (1991).
16. J. R. Sporre, "Diagnosis of the flux emanating from the intermediate focus of an extreme ultraviolet light lithography source," PhD Thesis, University of Illinois at Urbana-Champaign (2013).

Daniel T. Elg is a doctoral student at the Center for Plasma-Material Interactions at the University of Illinois at Urbana-Champaign. He received his BS degree in electrical and computer engineering from Olin College in 2011 and his MS degree in nuclear, plasma, and radiological engineering from the University of Illinois in 2013. He is a student member of SPIE. His research interests include plasma physics and plasma processing applications.

John R. Sporre is an RIE process engineer at IBM developing methods for next-generation semiconductor manufacturing. His past areas of research have included energetic plasma ion and neutral characterization, laser-assisted plasma formation, as well as plasma-based surface manipulation.

Davide Curreli is an assistant professor of nuclear, plasma, and radiological engineering at the University of Illinois at Urbana-Champaign, and is affiliated with the Center for Plasma-Material Interactions. His main focus is on plasma modeling and plasma code development for industrial and nuclear fusion applications.

Ivan A. Shchelkanov is a postdoctoral research associate at the Center for Plasma-Material Interactions, having joined the University of Illinois at Urbana-Champaign in 2013. He received his specialist degree and PhD degree from the Plasma Physics Department at Moscow Engineering Physical Institute (MEPhI). His research interest is technological implementation of cold plasma processing.

David N. Ruzic is the Abel Bliss professor of nuclear, plasma, and radiological engineering and director of the Center for Plasma Material Interactions at the University of Illinois at Urbana-Champaign. He is a fellow of the American Nuclear Society, the American Vacuum Society (AVS), and the Hertz Foundation. He also serves as the scientific director for the International Union of Vacuum Science, Techniques, and Applications.

Karl R. Umstadter is a system design engineer at KLA-Tencor. He is an AVS plasma applications board member and sits on the ANSI Z136 Accredited Standards Committee for Laser Safety. His background includes plasma physics, laser-materials interactions, vacuum science, and diagnostics development. Currently, he is active in semiconductor technology inspection and review systems architecture design.